

# Microstructure and Mechanical Properties of CoCrFeNi(Ti-Al) High Entropy Alloys

Ilkay Kalay 

Cankaya University, Department of Materials Science and Engineering, Ankara, Turkey

## ABSTRACT

The structure and mechanical properties of CoCrFeNi and CoCrFeNiTi<sub>0.5</sub>Al<sub>0.5</sub> (in molar ratio) high entropy alloys were investigated using X-ray diffraction (XRD), optical microscope (OM), scanning electron microscope (SEM), hardness and compression tests. With the addition of Ti and Al, the crystal structure of CoCrFeNi changed from FCC to a mixture of FCC and double BCC structures. The lattice parameter of FCC increases upon addition of Al and Ti. The microstructure analysis shows the morphological transition of dendrites from non-equiaxed to equiaxed during the suction casting of CoCrFeNiTi<sub>0.5</sub>Al<sub>0.5</sub> alloy. The Vickers microhardness testing of CoCr-FeNi alloy reveals significant increase in hardness with the addition of Al and Ti. The hardness values are improved in as-suction cast CoCrFeNi and CoCrFeNiTi<sub>0.5</sub>Al<sub>0.5</sub> alloys compared to their as-cast alloys due to strengthening. The CoCrFeNiTi<sub>0.5</sub>Al<sub>0.5</sub> alloy yields at 1997 MPa and fails at 2344 MPa. The fracture mechanism of CoCrFeNiTi<sub>0.5</sub>Al<sub>0.5</sub> alloy reveals a cleavage mode.

### Keywords:

High entropy alloys; Microstructure; Microhardness; Compression test; Metallic alloys.

## INTRODUCTION

Attributed to the combinations of their unique and remarkable properties such as superior high temperature strength, high strength, high hardness, outstanding magnetic properties, excellent oxidation and corrosion resistance, high entropy alloys (HEAs) have attracted much attention [1-5]. Since the proposed concept of HEA by Cantor and et al. [1] and Yeh and et al. [2-4], a number of HEAs, such as the single phase solid solution HEAs, multiphase solid solution HEAs, refractory HEAs [5], amorphous HEAs [6], light weight HEAs [7] and magnetic HEAs [8] have been identified. HEAs were originally expressed as solid solutions composed of five or more principal metallic elements taken into equiatomic or nearly equiatomic proportions between 5 and 35 at.%. The liquid or random solid solutions of the alloys have higher entropy of mixing. Besides principal elements, these alloys can include secondary elements with compositions less than 5 at.%. Even HEAs have typically at least 5 constituent elements, they have simple crystal structures such as face centered cubic (FCC) [9-11], body centered cubic (BCC) [12-14] or hexagonal centered cubic (HCP) [15-17]. However, the HEAs concept has been developed recently as many HEAs have complex multiphase structures rather than a

single crystal structure. There are four core effects determined related to the formation of HEAs. These effects can be given as the high entropy, severe-lattice distortion, sluggish diffusion and cocktail effects. Yang and Zhang [18] proposed other important factors are the ratio of mixing entropy,  $\Delta S_{mix}$  to the mixing enthalpy,  $\Delta H_{mix}$ , that is  $(\frac{\Delta S_{mix}}{\Delta H_{mix}}) = \Omega$ , atomic size difference,  $\delta$ , and valance electron concentrations (VEC). They reported that HEAs can be produced in case  $\Omega \geq 1.1$  and  $\delta \leq 6.6\%$ .  $\Delta H_{mix}$  and  $\Delta S_{mix}$  can be expressed as:

$$\Delta H_{mix} = \sum_{i=1, j \neq i}^n \Omega_{ij} c_i c_j \quad (1)$$

and

$$\Delta S_{mix} = -R \sum_i^n c_i \ln c_i \quad (2)$$

where  $\Omega_{ij} = 4\Delta H_{AB}$  for binary systems, R is the gas constant,  $c_i$  is the atomic percent of  $i^{\text{th}}$  element. VEC is

$$VEC = \sum_i^n c_i (VEC)_i \quad (3)$$

Here,  $(VEC)_i$  is the valance electron concentration of  $i^{\text{th}}$  element. VEC is a critical parameter for designing

### Article History:

Received: 2020/04/16

Accepted: 2020/06/17

Online: 2020/06/26

Correspondence to: Ilkay Kalay, Cankaya University, Materials Science and Engineering, 06790, Ankara, TURKEY  
E-Mail: ikalay@cankaya.edu.tr  
Phone: +90 312 233 1394  
Fax: +90 312 233 1026

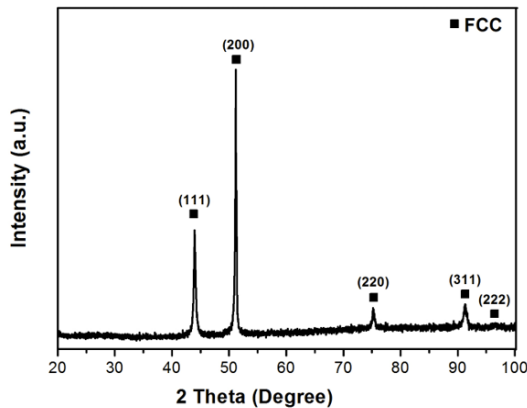


Figure 1. XRD pattern of as-cast CoCrFeNi alloy.

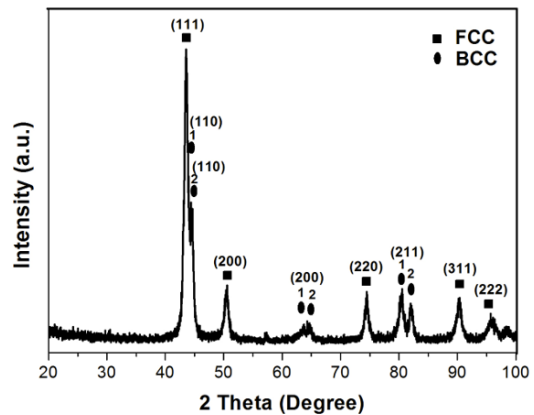


Figure 2. XRD pattern of as-cast CoCrFeNiTi<sub>0.5</sub>Al<sub>0.5</sub> alloy.

the compositions of HEAs that relates the structure and strength and ductility. Previous studies reported that when  $VEC > 8.0$ , the FCC solid solution is stable, when  $VEC < 6.87$ , the BCC solid solution is stable and when  $6.87 \leq VEC < 8.0$ , the structure of HEA will be multiphase consisted of FCC and BCC [19]. Furthermore, HEAs may also contain the coexistence of ordered and disordered forms of the same structure. The presence of BCC and ordered BCC (B2) phases together [20-22] and the coexistence of FCC and ordered FCC ( $L1_2$ ) phases [23] were reported previously.

In particular, CoCrFeNi HEA has attracted much attention attributed to its outstanding fracture toughness and ductility [24-26]. However, its poor strength values restrict their potential applicability as structural materials. Recently, Liu et al. [27] reported the tensile strength of 1.2 GPa and tensile strain of 18.9% when Mo is added to CoCrFeNi HEAs. Subsequently, Lu et al. [28] proposed that AlCoCrFeNi<sub>2.1</sub> alloy exhibits a fracture tensile strength of 944-1050 MPa and tensile strain of 17%-25.6%. The work reported here is aimed to investigate the effect of Ti and Al on the structure and mechanical properties of CoCrFeNi HEA and concentrated on CoCrFeNiTi<sub>0.5</sub>Al<sub>0.5</sub> alloy using several characterization techniques including XRD, OM, SEM, hardness and compression tests.

## MATERIAL AND METHODS

The alloy ingots with nominal compositions of CoCrFeNi and CoCrFeNiTi<sub>0.5</sub>Al<sub>0.5</sub> alloys were produced by Edmund Bühler MAM-1 vacuum arc melter with turbomolecular pumping system HVT52/G using highly pure elements (0.999 Al, Ti, Ni, Fe, Cr and Co, by weight) in the bulk form under an Ar atmosphere. The alloy ingots with a mass of 3-5 g were reprocessed three times to ensure homogeneity. The ingots were then cast into copper molds with diameters of 3 mm via suction casting to obtain higher cooling rates during solidification. The effects of

cooling rate during suction casting on microstructure and mechanical properties were also investigated. The structural analysis of the as-cast and suction-cast alloys was carried out by D8 Advance Bruker X-ray Diffractometer using Cu-K $\alpha$  radiation ( $\lambda=1.5406 \text{ \AA}$ ). The tube voltage and current of diffractometer were 40 kV and 30 mA, respectively. The diffraction data were collected in a diffraction angle range from 20° to 100° with a scanning rate of 0.5°/min. XRD analysis was carried out on the bulk form of rod specimens which were initially ground to remove any oxide layer. The microstructural analysis of the alloys was performed using Nikon Eclipse LV150 digital camera Optical microscope and FEI Nova NanoSEM 430 Scanning electron microscope. The Nova NanoSEM 430 operated at 20-30 kV. The OM and SEM specimens were initially ground, polished and etched using a mixture of 67 vol. % methanol and 33 vol. % nitric acid (HNO<sub>3</sub>) solution. The SEM imaging was performed in secondary electron mode. Compression tests were carried out using MTS Criterion Model 45 universal testing machine (100 kN) to investigate the yield and compressive strengths of CoCrFeNiTi<sub>0.5</sub>Al<sub>0.5</sub> alloy. During compression tests, the gauge dimensions of the specimens were adjusted to be  $3.0 \pm 0.3 \text{ mm}$  in diameter and  $6.0 \pm 0.3 \text{ mm}$  in length to keep an aspect ratio of 2:1. The crosshead speed and strain rate were chosen as 0.03 mm/min and  $10^{-4} \text{ s}^{-1}$ , respectively. The fractography analysis was carried out using OM and SEM. The hardness tests were carried out using InnovaTest Nexus 7501 Universal Hardness Tester. The Vickers micro-hardness tests due to ASTM standard E92 were performed using a test load of 10 kgf with a dwell time of 10 s. At least 10 indentations were performed for each specimen. The Vickers Hardness (HV) values were also converted into MPa by multiplying by 9.807.

## RESULTS AND DISCUSSION

The  $\Delta H_{\text{mix}}$ ,  $\Delta S_{\text{mix}}$  and VEC values of CoCrFeNi and CoCrFeNiTi<sub>0.5</sub>Al<sub>0.5</sub> and alloys were calculated using equ-

**Table 1.** Thermodynamic data of the alloys.

Alloy	$\Delta H_{mix}$ (J/mol)	$\Delta S_{mix}$ (J/mol.K)	VEC
CoCrFeNi	-3.78	11.53	8.25
CoCrFeNiTi <sub>0.5</sub> Al <sub>0.5</sub>	-15.52	14.53	7.29

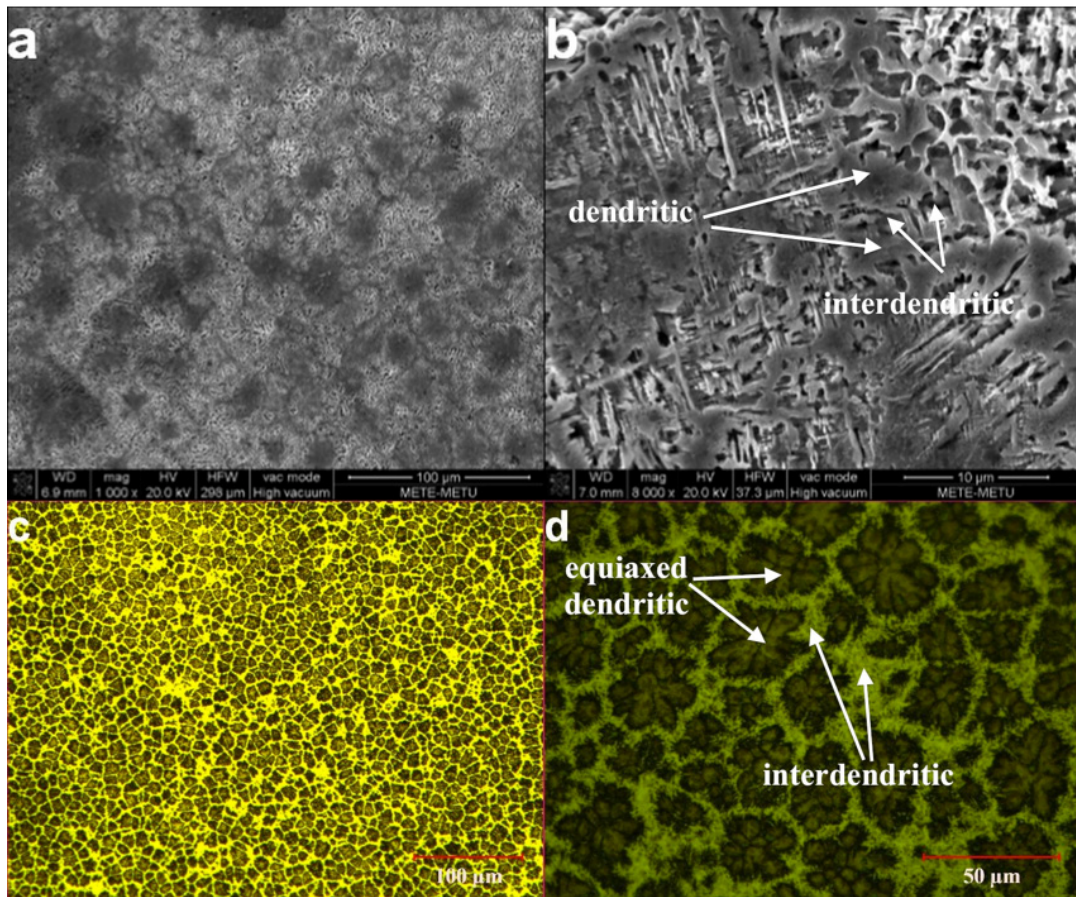
ations (1), (2) and (3), respectively and tabulated in Table 1. The expected crystal structures based on calculated VEC values are FCC for CoCrFeNi and FCC+BCC for CoCrFeNiTi<sub>0.5</sub>Al<sub>0.5</sub> alloy. Fig. 1 indicates the XRD diffractogram of CoCrFeNi alloy. It is clear that as-cast CoCrFeNi alloy shows only the diffraction peaks associated with FCC phase as expected from VEC calculations. Fig. 2 indicates the XRD pattern of CoCrFeNiTi<sub>0.5</sub>Al<sub>0.5</sub> alloy. It is observed that the new diffraction peaks corresponding to BCC phases appear with the addition of Al and Ti. XRD analysis of CoCrFeNiTi<sub>0.5</sub>Al<sub>0.5</sub> alloy reveals the existence of FCC + double BCC (BCC<sub>1</sub> and BCC<sub>2</sub>) structure. The lattice parameters (a) of the corresponding BCC and FCC structures were calculated from the indexed XRD patterns. The lattice parameters were determined using the combination of Bragg's Law ( $\lambda = 2d \sin \theta$ ), where  $\lambda=1.5406 \text{ \AA}$  for CuK $\alpha$  radiation,  $\theta$  is the Bragg's angle, d is the interplanar spacing and d-spacing equation

**Table 2.** Lattice parameters of the main constituent phases of the alloys.

Alloy	$a_{FCC}$ (nm)	$a_{BCC(1)}$ (nm)	$a_{BCC(2)}$ (nm)
CoCrFeNi	0.357 $\pm 0.0005$	-	-
CoCrFeNiTi <sub>0.5</sub> Al <sub>0.5</sub>	0.360 $\pm 0.0009$	0.293 $\pm 0.0009$	0.288 $\pm 0.0005$

for cubic structures ( $\frac{1}{d^2} = \frac{h^2 + k^2 + l^2}{a^2}$ ), where h, k, l are the indices of the corresponding planes). Table 2 tabulates the lattice parameters of the corresponding crystal structures of the alloys. The lattice parameter of the FCC structure in the CoCrFeNi alloy was determined as 0.357 nm, based on the interplanar spacing of peaks from XRD pattern. The corresponding lattice parameters of FCC, BCC<sub>1</sub> and BCC<sub>2</sub> phases in CoCrFeNiTi<sub>0.5</sub>Al<sub>0.5</sub> alloy were determined as 0.360 nm, 0.293 nm and 0.288 nm, respectively. The lattice parameter of FCC increases with the further addition of Al and Ti. Al and Ti have the largest atomic size in the system therefore distortions and enlargement occur in the crystal lattice of CoCrFeNiTi<sub>0.5</sub>Al<sub>0.5</sub>.

The SEM images of as-cast CoCrFeNiTi<sub>0.5</sub>Al<sub>0.5</sub> alloy are presented in Fig. 3 (a, b). The microstructure of the as-

**Figure 3.** (a-b) SEM images of as cast CoCrFeNiTi<sub>0.5</sub>Al<sub>0.5</sub> alloy, (c-d) OM images of as suction cast 3 mm diameter CoCrFeNiTi<sub>0.5</sub>Al<sub>0.5</sub> rod.

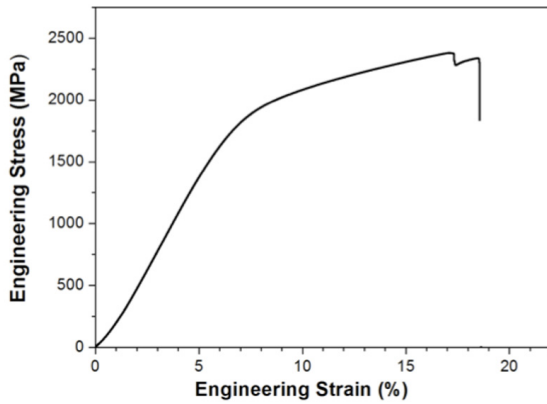


**Figure 4.** The compressive stress-strain curve of CoCrFeNiTi<sub>0.5</sub>Al<sub>0.5</sub> alloy at room temperature.

cast CoCrFeNiTi<sub>0.5</sub>Al<sub>0.5</sub> alloy exhibits two distinct regions; dendritic and interdendritic, which are typical of many HEAs after casting. It is clear that even within the dendritic and interdendritic regions, contrast differences are observed due to the variable chemical compositions. Fig. 3 (c, d) indicate the optical microscope images of 3 mm diameter suction-cast CoCrFeNiTi<sub>0.5</sub>Al<sub>0.5</sub> alloy. The micrographs

show the dendritic and interdendritic structures. It should be noted that Al is a strongest stabilizer of the BCC structure leading to the formation dual BCC modulated microstructure in CoCrFeNiTi<sub>0.5</sub>Al<sub>0.5</sub> system. By the addition of Al, complete FCC structure changes to FCC+BCC structures. With the addition of Ti, dual BCC phase were observed in CoCrFeNiTi<sub>0.5</sub>Al<sub>0.5</sub> alloy. Fig. 3 (a-d) reveals that the structure of dendrites has also been changed from non-equiaxed dendritic grain to equiaxed dendritic grains during suction casting of the alloy.

The compressive engineering stress-strain diagram of CoCrFeNiTi<sub>0.5</sub>Al<sub>0.5</sub> alloy is given in Fig. 4. The compressive yield strength and the fracture strength were determined as 1997 MPa and 2344 MPa, respectively. Wang et al. [29] reported the yield stress and compressive strength as 1250.96 MPa and 2004.23 MPa, respectively for AlCoCrFeNi alloy. Our findings for CoCrFeNiTi<sub>0.5</sub>Al<sub>0.5</sub> alloy show that the yield strength and compressive strength values are enhanced by the addition of Ti compared to that of AlCoCrFeNi alloy [29]. The microhardness test results were determined as 107±5 HV (1049±49.0 MPa) and 134±22 HV (1314±215.8

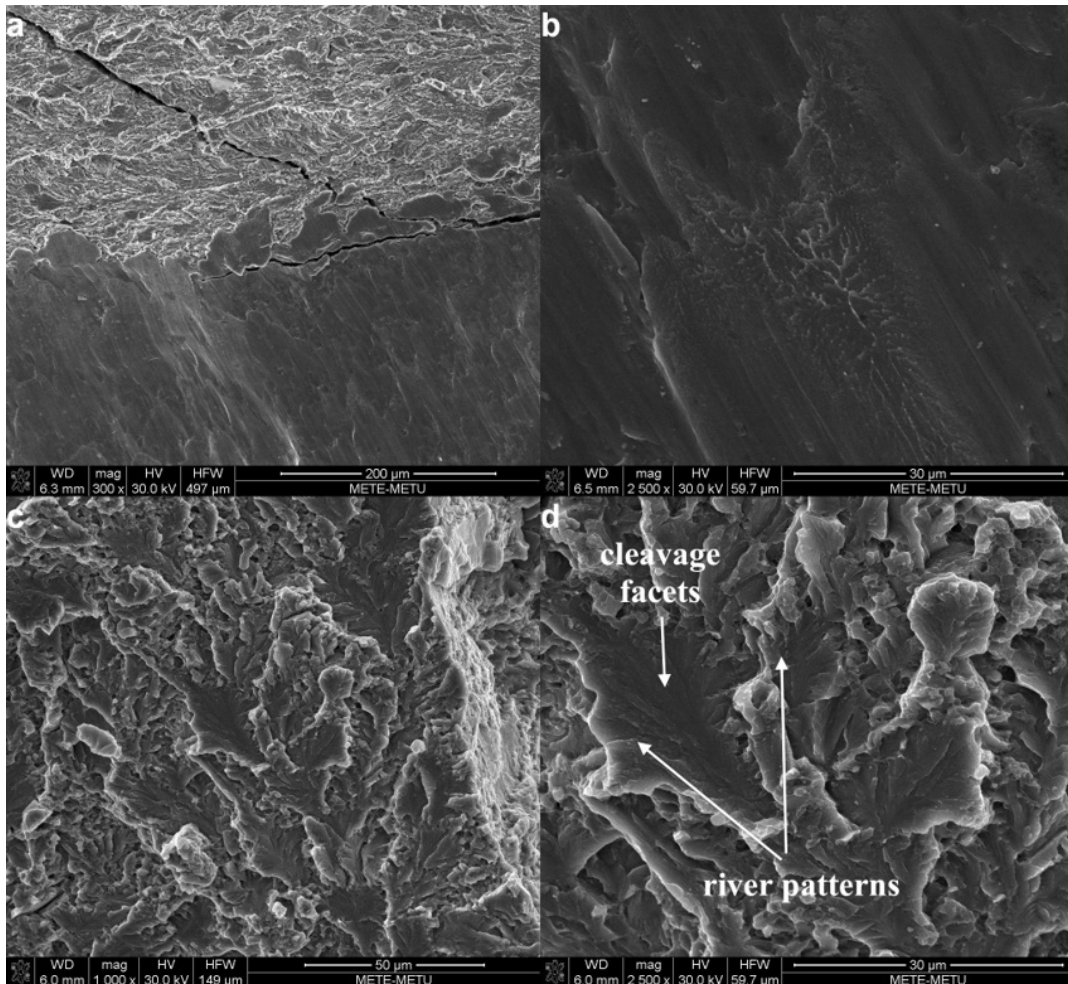


**Figure 5.** (a-d) SEM micrographs of fractured surfaces of CoCrFeNiTi<sub>0.5</sub>Al<sub>0.5</sub> alloy.

MPa) for as-cast and as-suction cast CoCrFeNi HEAs, respectively. The hardness values were determined as  $488 \pm 15$  HV ( $4786 \pm 147$  MPa) and  $647 \pm 14$  HV ( $6345 \pm 137.3$  MPa) for as-cast and as-suction cast CoCrFeNiTi<sub>0.5</sub>Al<sub>0.5</sub> alloys, respectively. The hardness value is increasing significantly with the addition of Al and Ti due to the change in crystal structure from FCC in CoCrFeNi alloy to FCC + double BCC in CoCrFeNiTi<sub>0.5</sub>Al<sub>0.5</sub> alloy. The formation of BCC phase creates an interface between FCC and BCC structures therefore the dislocation movement is hindered and due to strengthening, the hardness of the alloy is improved. Furthermore, the lattice distortion due to the formation of BCC structure also increases the activation energy of dislocation motion. This results in solid solution strengthening and thus increases the hardness of the alloy. The as-suction cast CoCrFeNiTi<sub>0.5</sub>Al<sub>0.5</sub> alloy has higher hardness value than its as-cast alloy. CoCrFeNi alloy also has the same trend. This is mainly caused by the change in cooling rate and thus the microstructure of the produced alloy during suction casting. The reduction in grain size by increasing cooling rate improves the strength of the suction cast alloy.

SEM micrographs of the fractured surface of CoCrFeNiTi<sub>0.5</sub>Al<sub>0.5</sub> are illustrated in Fig. 5. The fractured surface of CoCrFeNiTi<sub>0.5</sub>Al<sub>0.5</sub> alloy shows a typical cleavage fracture implying a brittle character. The surface of the alloys reveals the cleavage facets and river patterns. It is clear that the patterns are propagating along either the grain boundaries or transgranular cleavage planes. Cleavage or quasi-cleavage features are generally observed on the fracture surface HEAs with BCC or BCC+FCC structures [42].

## CONCLUSION

The structure and mechanical properties of CoCrFeNi and CoCrFeNiTi<sub>0.5</sub>Al<sub>0.5</sub> HEAs were examined using XRD, OM, SEM, compressive fracture and hardness testing. The alloys were prepared via vacuum arc melting and the alloy rods were synthesized by suction casting technique. With the addition of Ti and Al to CoCrFeNi HEA, the crystal structure has changed from FCC to a mixture of double BCC (BCC<sub>1</sub> and BCC<sub>2</sub>) and FCC structures. The hardness values were also increased by the addition of Al and Ti. Furthermore, the suction-cast CoCrFeNiTi<sub>0.5</sub>Al<sub>0.5</sub> alloy exhibited the higher hardness value compared to its as-cast alloy due to the grain refinement by rapid cooling during suction casting operation. The compression test revealed that CoCrFeNiTi<sub>0.5</sub>Al<sub>0.5</sub> high entropy alloy yields at 1997 MPa and resists up to 2344 MPa. SEM analysis of fractured surface of CoCrFeNiTi<sub>0.5</sub>Al<sub>0.5</sub> alloy reveals a cleavage mode.

## References

1. Cantor B, Chang ITH, Knight P, Vincent AJB. Microstructural development in equiatomic multicomponent alloys. *Materials Science and Engineering A* 375–377 (2004) 213–218.
2. Yeh JW, Chen YL, Lin SJ, Chen SK. High-Entropy Alloys – A New Era of Exploitation. *Materials Science Forum* 560 (2007) 1–9.
3. Yeh JW, Chen SK, Lin SJ, Gan JY, Chin TS, Shun TT, Tsau CH, Chang SY. Nanostructured high-entropy alloys with multiple principal elements: Novel alloy design concepts and outcomes. *Advanced Engineering Materials* 6 (2004) 299–303.
4. Wu JM, Lin SJ, Yeh JW, Chen SK, Huang YS, Chen HC. Adhesive wear behavior of AlxCoCrCuFeNi high-entropy alloys as a function of aluminum content. *Wear* 261 (2006) 513–519.
5. Senkov ON, Miracle DB, Chaput KJ, Couzinie JP. Development and exploration of refractory high-entropy alloys—a review. *Journal of Materials Research* 33 (2018) 3192–3133.
6. Hu Q, Guo S, Wang J, et al. Parametric Study of Amorphous High-Entropy Alloys formation from two New Perspectives: Atomic Radius Modification and Crystalline Structure of Alloying Elements. *Science Reports* 7 (2017) 39917.
7. Feng R, Gao MC, Lee C, Mathes M, Zuo T, Chen S, Hawk JA, Zhang Y, Liaw PK. Design of Light-Weight High-Entropy Alloys. *Entropy* 18 (2016) 333.
8. Lucas MS, Mauger L, Muñoz JA, Xiao Y, Xiao Y, Sheets AO, Semiatin SL, Horwath J, Turgut Z. Magnetic and vibrational properties of high-entropy alloys. *Journal of Applied Physics* 109 (2011) 07E307.
9. Gali A, George E. P. Tensile properties of high- and medium-entropy alloys. *Intermetallics* 39 (2013) 74–78.
10. Tsai KY, Tsai MH, Yeh JW. Sluggish diffusion in Co–Cr–Fe–Mn–Ni high-entropy alloys. *Acta Mater.* 61 (2013) 4887–4897.
11. Liu WH, Wu Y, He JY, Nieh TG, Lu ZP. Grain growth and the Hall-Petch relationship in a highentropy FeCrNiCoMn alloy. *Scr. Mater.* 68 (2013) 526–529.
12. Senkov ON, Woodward CF. Microstructure and properties of a refractory NbCrMo<sub>0.5</sub>Ta<sub>0.5</sub>TiZr alloy. *Mater. Sci. Eng. A* 529 (2011) 311–320.
13. Senkov ON, Wilks GB, Scott JM, Miracle DB. Mechanical properties of Nb<sub>25</sub>Mo<sub>25</sub>Ta<sub>25</sub>W<sub>25</sub> and V<sub>20</sub>Nb<sub>20</sub>Mo<sub>20</sub>Ta<sub>20</sub>W<sub>20</sub> refractory high entropy alloys. *Intermetallics* 19 (2011) 698–706.
14. Senkov ON, Scott JM, Senkova SV, Miracle DB, Woodward CF. Microstructure and room temperature properties of a high-entropy TaNbHfZrTi alloy. *J. Alloys. Compd.* 509 (2011) 6043–6048.
15. Takeuchi A, Amiya K, Wada T, Yubuta K, Zhang W. High-entropy alloys with a hexagonal close-packed structure designed by equiatomic alloy strategy and binary phase diagrams. *JOM* 66 (2014) 1984–1992.
16. Feuerbacher M, Heidelmann M, Thomas C. Hexagonal high-entropy alloys. *Mater. Res. Lett.* 3 (2015) 1–6.
17. Zhao YJ et al. A hexagonal close-packed highentropy alloy: the effect of entropy. *Mater. Des.* 96 (2016) 10–15.
18. Yang X, Zhang Y. Prediction of high-entropy stabilized solid-solution in multi-component alloys. *Materials Chemistry and Physics* 132 (2–3) (2012) 233–238.
19. Guo S, Ng C, Lu J, Liu CT. Effect of valence electron concentration on stability of fcc or bcc phase in high entropy alloys. *Journal of Applied Physics* 109 (2011) 103505.

20. Singh S, Wanderka N, Murty BS, Glatzel U, Banhart J. Decomposition in multi component AlCoCrCuFeNi high-entropy alloy. *Acta Materialia* 59 (2011) 182-190.
21. Tsai MH, Yuan H, Cheng G, Xu W, Jian WW, Chuang MH, Juan CC, Yeh AC, Lin SJ, Zhu Y. Significant hardening due to the formation of a sigma phase matrix in a high entropy alloy. *Intermetallics* 33 (2013) 81-86.
22. Tong CJ, Chen YL, Chen SK, Yeh JW, Shun TT, Tsau CH, Lin SJ, Chang SY. Microstructure characterization of AlxCoCrCuFeNi high-entropy alloy system with multiprincipal elements. *Metallurgical Materials and Transactions A* 36 (2005) 881-893.
23. Tsai MH, Yuan H, Cheng G, Xu W, Tsai KY, Tsai CW, Jian WW, Juan CC, Shen WJ, Chuang MH, Yeh JW, Zhu YT. Morphology, structure and composition of precipitates in Al<sub>0.3</sub>CoCrCu<sub>0.5</sub>FeNi high-entropy alloy. *Intermetallics* 32 (2013) 329-336.
24. Meshkov II, Novoselov EA, Shapeev AV, Yanilkin AV. Sublattice formation in CoCrFeNi high-entropy alloy. *Intermetallics* 112 (2019) 106542.
25. Wang B, Haiyan H, Naeem M, et al. Deformation of CoCrFeNi high entropy alloy at large strain. *Scripta Materialia* 115 (2018) 54-57.
26. Guo S, Ng C, Wang Z, Liu CT. Solid solutioning in equiatomic alloys: limit set by topological instability. *Journal of Alloys and Compounds* 583 (2014) 410-413.
27. Liu WH, Lu ZP, He JY, Luan JH, Wang ZJ, Liu B, Liu Y, Chen MW, Liu CT. Ductile CoCrFeNiMox high entropy alloys strengthened by hard intermetallic phases. *Acta Materialia* 116 (2016) 332-342.
28. Lu Y. P., Gao X., Jiang L., Chen Z., et al. Directly cast bulk eutectic and near-eutectic high entropy alloys with balanced strength and ductility in a wide temperature range. *Acta Materialia* 214 (2017) 143-150.
29. Wang YP, Li BS, Ren MX, Yang C, Fu HZ. Microstructure and compressive properties of AlCrFeCoNi high entropy alloy. *Materials Science and Engineering: A* 491 (2008) 154-158.